Expert Systems With Applications 296 (2026) 129045

Contents lists available at ScienceDirect

Expert Systems With Applications

journal homepage: www.elsevier.com/locate/eswa

Quantum Metabolic Avatar: A digital replica of metabolism enhanced by quantum algorithms

A. Abeltino [a,1], C. Serantoni [a,b,1], M.M. De Giulio [a], A. Riente [a], S. Capezzone [c], R. Esposito [d], M. De Spirito [a,b], G. Maulucci [a,b,*]

[a] Metabolic Intelligence Lab, Neuroscience, Università Cattolica del Sacro Cuore, Largo Francesco Vito 1, 00168 Rome, Italy
[b] Physics for life Science, Fondazione Policlinico Universitario Agostino Gemelli IRCCS, Rome, Italy
[c] Gruppo Fastal Blu Sistemi, Via Nomentana 263, 00161 Rome, Italy
[d] Digital Innovation Hub Roma, Chirale S.r.l., Via Ignazio Persico 32-46, 00154 Rome, Italy

ARTICLE INFO

Keywords:
Quantum machine learning
Quantum computing
Pma
QMA
Echo state network
Quantum echo state network

ABSTRACT

The integration of quantum computing (QC) into predictive modeling represents a transformative advancement in machine learning, providing substantial improvements over traditional methods. This study compares classical Echo State Networks (ESN) with quantum Echo State Networks (qESN) for time-series forecasting, emphasizing the concept of a metabolic avatar—a dynamic data-driven model of individual metabolic processes. Utilizing time-series data from six distinct users, we assessed both models' precision and adaptability through Root Mean Squared Error (RMSE).

Our results demonstrate consistent superiority of qESN over classical ESN, highlighted by a 30% RMSE reduction during cross-validation (CV). Notably, qESN showed remarkable stability and accuracy even with limited training data, underscoring its effectiveness in data-sparse scenarios. Furthermore, we examined model performance in datasets containing outliers. QESN significantly outperformed classical ESN, achieving approximately 76% lower RMSE in CV and about 55% lower RMSE in walk-forward validation (WFV). This demonstrates qESN's enhanced robustness and reduced susceptibility to overfitting.

Crucially, our findings highlight the Quantum Metabolic Avatar's (QMA) profound potential for personalized predictive analytics, essential for applications in personalized healthcare and customized wellness programs. The study strongly supports integrating quantum algorithms into predictive modeling, marking a pivotal advancement towards highly personalized and dynamic metabolic avatars.

1. Introduction

In the rapidly evolving landscape of quantum computing (QC), the integration of machine learning algorithms presents a transformative opportunity to tackle challenges that have long persisted in modeling temporal dynamics (Biamonte et al., 2017). One promising development in this direction is the emergence of quantum Echo State Networks (qESN) (Liu et al., 2020), a class of models that leverage a reservoir based on a quantum register to process sequential information efficiently. The appeal of qESNs lies in their ability to utilize quantum superposition, entanglement, and the naturally high-dimensional structure of quantum state spaces to encode and retain temporal dependencies—capabilities that are often limited or computationally expensive in classical models.

At the conceptual core of qESNs is the framework of Quantum Reservoir Computing (QRC) (Fujii and Nakajima, 2021:; Suzuki et al., 2022), which enables the encoding of input time series into the dynamics of a quantum system with fading memory. This fading memory, an essential feature for many forecasting tasks where past information influences future states, is inherently present in quantum systems due to

Abbreviations: QMA, Quantum Metabolic Avatar; PMA, Personalized Metabolic Avatar; ESN, Echo State Network; qESN, quantum Echo State Network; RMSE, Root Mean Squared Error; EB, Energy Balance; CV, Cross-Validation; WFV, Walk-Forward Validation; QC, Quantum Computing; QRC, Quantum Reservoir Computing; SD, Standard Deviations; NISQ, Noisy Intermediate-Scale Quantum.

* Corresponding author at: Metabolic Intelligence Lab, Neuroscience, Università Cattolica del Sacro Cuore, Largo Francesco Vito 1, 00168, Rome, Italy.
E-mail address: giuseppe.maulucci@unicatt.it (G. Maulucci).

[1] These authors contributed equally.

https://doi.org/10.1016/j.eswa.2025.129045
Received 13 March 2024; Received in revised form 1 July 2025; Accepted 14 July 2025
Available online 15 July 2025

the time evolution of their state vectors. As such, QRC—and by extension qESNs—offer a means to capture both short- and long-range dependencies without the need for backpropagation or circuit optimization. These properties are especially attractive for applications that demand fast inference with minimal training, such as in embedded or personalized health systems.

Compared to other quantum neural models that require variational parameters and circuit training, qESNs stand out for their structural simplicity and computational efficiency. Their internal dynamics are fixed and disordered, eliminating the need to optimize quantum gates or layers during training. Remarkably, it has been shown that a qESN with as few as 5 qubits can match or even exceed the memory capacity of a classical Echo State Network with 500 nodes (Fujii and Nakajima, 2017; Molteni et al., 2023). This efficiency, combined with the exponential state-space growth intrinsic to quantum systems, makes qESNs ideal for scenarios in which classical models struggle—particularly under data scarcity or high noise conditions. Recent variants of the ESN architecture, such as those incorporating multiple delayed outputs (Yao et al., 2022) or fractional-integer orders (Yao et al., 2024), have attempted to address memory and prediction limitations in complex temporal tasks. However, unlike qESN, these models still rely on large state spaces, manual tuning of hyperparameters, or increased architectural complexity. In contrast, qESNs exploit quantum-enhanced dynamics to encode richer temporal dependencies without increasing the model complexity, offering a potentially more scalable and generalizable solution for noisy or data-scarce regimes.

One of the most persistent limitations in classical time-series modeling lies in the reliance on large, clean datasets. However, many real-world applications—including personalized health monitoring—are characterized by incomplete, sparse, or irregular data. These conditions can hinder the generalization ability of classical networks, often resulting in overfitting and unstable predictions. In this context, QC offers an alternative route. Several recent studies have demonstrated that quantum machine learning models are capable of learning effectively from limited datasets (Kobayashi et al., 2022), often showing enhanced resilience against data corruption and outliers compared to classical counterparts (Caro et al., 2022; Abeltino et al., 2023; Abeltino et al., 2022). These properties make qESNs particularly suitable for biomedical time-series forecasting, where sensor noise, variability among individuals, and missing values are common.

In this study, we propose the Quantum Metabolic Avatar (QMA), a novel application of qESN-based modeling to forecast weight changes in response to nutritional intake. QMA is a quantum-enhanced evolution of the Personalized Metabolic Avatar (PMA) (Abeltino et al., 2023; Abeltino et al., 2022; Bianchetti et al., 2022), a deep learning-based model built on Gated Recurrent Units (GRUs), previously designed to learn the metabolic response of individuals to macronutrient composition and energy balance. While PMA provided promising results in digital nutrition applications, its performance was limited when trained on sparse or noisy datasets. QMA addresses this limitation by leveraging the memory capacity and noise resilience of qESNs, enabling accurate predictions even when user-specific data are scarce or affected by irregularities.

The rationale for adopting qESNs instead of other quantum neural models lies in their architectural and computational advantages. Unlike parameterized quantum circuits or quantum perceptrons, qESNs require no circuit training and exhibit stable internal dynamics due to their fixed structure. This not only reduces the computational burden but also makes qESNs compatible with current Noisy Intermediate-Scale Quantum (NISQ) hardware. Their design aligns naturally with temporal forecasting tasks and offers improved robustness, generalization, and interpretability.

Throughout this work, we investigate how QMA performs under various conditions, including different lengths of training data, the presence of noise and outliers, and both cross-validation and walk-forward validation schemes. By comparing qESNs with their classical counterparts in these realistic settings, we aim to demonstrate that quantum-enhanced models can offer tangible benefits in biomedical forecasting—where adaptability, personalization, and resilience are essential. Ultimately, QMA provides not only a new tool for digital health modeling but also a compelling demonstration of how quantum computing can extend the boundaries of what is feasible with conventional machine learning.

2. Methods

2.1. Data Preparation and preprocessing

The dataset employed in this study was derived from six individual users monitored over variable time spans (ranging from 140 to 300 days), using our custom-built digital health interface, the ArMOnIApp (Bianchetti et al., 2022). This platform integrates self-reported dietary logs, structured food databases, and automatic measurements from wearable devices, including smart bands and smart scales (Table S1).

For each user, five time series were acquired on a daily basis:

- Energy Balance (EB), in kilocalories (kcal), computed as intake minus estimated expenditure,
- Weight, in kilograms (kg), measured via Bluetooth-enabled smart scales,
- Carbohydrate Intake, in grams (g),
- Protein Intake, in grams (g),
- Fat Intake, in grams (g).

These five features formed the input space for each time window used in prediction. Specifically, a 7-day look-back window was applied, resulting in a 35-dimensional input vector (5 variables $\times$ 7 days). The target variable for prediction was the body weight measured 7 days after the last input value (i.e., $w(t + 7)$).

Prior to modeling, the dataset underwent several preprocessing steps:

- Missing Value Handling: Days with incomplete logs were flagged and excluded from training. Time windows containing any null values were dropped to avoid interpolation bias. On average, this resulted in the exclusion of 8–12 % of total samples per user.
- Outlier Detection: Physiological plausibility filters were applied to eliminate data entries with implausible weight values (e.g., $>$180 kg or $<$ 40 kg) or extreme dietary logs (e.g., $>$8000 kcal/day). Additional experiments were conducted including controlled insertion of outliers to test model robustness (see section 3.3).
- Normalization: Each time series was normalized within-subject using z-score standardization:
- $z_i = \frac{x_i - \mu}{\sigma}$
- where μ and σ are the mean and standard deviation of the specific variable across that user's time series. This per-subject normalization preserves intra-individual variation while ensuring numerical stability across input ranges.
- Temporal Windowing: The final dataset was constructed by sliding a window of 7 days across the time series, generating overlapping input–output pairs with stride 1. Only complete windows with valid prediction labels (i.e., no missing $w(t + 7)$) were retained.

For further information refer to our previous studies (Abeltino et al., 2023; Abeltino et al., 2022; Abeltino et al., 2025).

2.2. Echo state network models

Two distinct models were developed: the classic ESN and its quantum implementation (qESN).

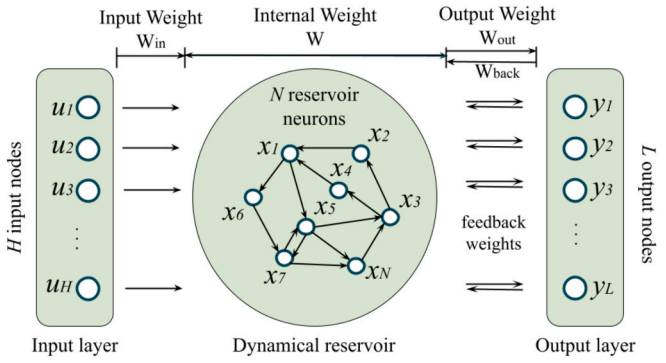

Fig. 1. ESN framework. The ESN comprises three primary components: input (u), internal state (x), and output (y). The input serves as the network's entry point for data or information to be processed. The internal state represents the network's memory, retaining past information and influencing the network's responses to current inputs. Finally, the output generates the network's response or prediction based on the processed information from the internal state. ESNs utilize this framework to effectively analyze temporal sequences, leveraging past information stored in the internal state to produce accurate predictions or outputs.

2.2.1. Classic Echo state network (ESN)

The classic ESN (Cui et al., 2012; Ma et al., 2016) was implemented using a network of interconnected nodes, forming a reservoir (Fig. 1).

Two critical hyperparameters, namely the 'spectral radius' and 'reservoir size', were utilized in its implementation. This model harnesses the reservoir's nonlinear transformation capabilities to map input data into a higher-dimensional space. Subsequently, a linear readout layer is employed to facilitate predictions.

When applied to a classical time series prediction scenario, an ESN operates on a sequence of historical data comprising inputs and their corresponding outputs. The primary objective for the ESN is to comprehend the relationship between past inputs and outputs. By learning from this historical context, the ESN aims to predict future outputs within the time series. qESN is composed by three main blocks:

- *Input*: The inputs consist of a sequence of values, such as past time measurements or time-related features. These inputs are represented as a vector. In our specific application, we incorporate 5 time series data sets (EB, Weight, Carbohydrates, Proteins and Fats), each reflecting a 7-day retrospective analysis. Consequently, our input is represented as a vector containing 5x7 = 35 elements.
- *Output*: The outputs are values corresponding to future measurements or future predictions we want to make. These are also represented as a vector. In our application we have only one output (Weight).
- *Operation*: The ESN comprises an input layer, a reservoir (or hidden layer), and an output layer. During training, inputs are fed into the input layer and propagated through the reservoir via randomly weighted connections. The state of the reservoir is updated based on the inputs and its previous state. Subsequently, a learning algorithm is used to adapt the weights between the reservoir and the output layer so that the ESN can approximate the relationship between the inputs and the desired outputs.

Mathematically, the update of the reservoir state can be represented as:

$$x(t) = f(W_{in}u(t) + W_{res}x(t-1))$$

where:

- $x(t)$ is the state of the reservoir at time t.
- f is a nonlinear activation function (typically a hyperbolic tangent).
- W_{in} is the input weight matrix.
- $u(t)$ is the input vector at time t
- W_{res} is the reservoir weight matrix.

2.2.2. Quantum Echo state Network

The qESN extends the classical ESN paradigm by integrating quantum computing principles. It uses amplitude encoding to map classical input vectors into quantum states, which are subsequently processed through a quantum circuit to extract dynamic features. A classical readout layer—implemented as a linear regression model—is then used to perform the final prediction.

As in the classical case, the qESN is composed of three main components: an input layer, a reservoir (implemented as a quantum circuit), and an output layer. Inputs consist of sequences of temporal values that are encoded into quantum states. Outputs represent the predicted future values, as in the classical case.

The reservoir performs the core computation through the evolution of quantum states, according to the following steps:

1. Input Vector Expansion: The input vector is expanded into a polynomial representation to increase dimensionality, matching the number of required quantum amplitudes.
2. Quantum Reservoir Amplitude Encoding: The expanded and normalized input vector is then used to initialize the quantum state across the qubit register. Normalization is essential to ensure the quantum state conforms to the unit-norm condition.
3. Quantum Circuit Execution: The quantum circuit is executed using a quantum simulator. During execution, measurements are performed on all qubits to extract probability amplitudes from the quantum reservoir.
4. Probability Processing: Measurement results are processed to calculate the probability distribution over the computational basis, reflecting the quantum system's final state.
5. Quantum Feature Vector Construction: By repeating the process across input samples, a quantum feature vector is generated for each instance. These vectors encode the temporal structure of the input sequence in a non-classical representation.

To define the quantum reservoir used in our qESN implementation, we designed a fixed-depth, parameterized quantum circuit capable of processing amplitude-encoded inputs over multiple qubits. In this study, we used a 4-qubit register, which offers a balance between representational capacity and simulation efficiency on classical hardware. Each input, originally consisting of 35 features (7-day window × 5 variables), was first expanded to 66 dimensions using a second-degree polynomial expansion, and then normalized for amplitude encoding.

The main architectural and operational parameters of the quantum reservoir are:

- Number of qubits: 4
- Encoding scheme: Amplitude encoding with input normalization
- Input expansion: Polynomial basis of degree 2 (resulting in 66 input dimensions)
- Circuit depth: 3 layers
- Entanglement scheme: Controlled-RY gates connecting all adjacent qubits at each layer
- Rotation gates: Parametric RX and RZ rotations applied to each qubit, derived from the input vector
- Measurement: Full measurement in the computational basis, resulting in a 16-dimensional output vector (2^4 basis states)
- Quantum features: The 16-dimensional probability vector serves as the quantum feature representation

The quantum circuit was implemented using Qiskit (v0.45.1) and executed on a statevector simulator to ensure reproducibility and scalability across experiments. All circuit parameters, including gate

Table 1
RMSE comparison for classic and qESN for single prediction, CV, and WFV. Mean average values are displayed alongside their respective standard deviations (SD).

User number	RMSE Classic CV	RMSE Quantum CV	RMSE Classic WFV	RMSE Quantum WFV
0	1.12 ± 0.44	0.70 ± 0.15	0.54	0.57
1	1.62 ± 1.10	0.79 ± 0.12	0.64	0.74
2	1.08 ± 0.88	0.64 ± 0.19	0.42	0.49
3	0.86 ± 0.20	0.72 ± 0.14	0.54	0.62
4	1.15 ± 0.38	0.81 ± 0.19	0.72	0.68
5	1.22 ± 0.55	1.15 ± 0.49	0.72	1.02

configuration and entanglement topology, were kept fixed across users to maintain experimental consistency.

A schematic representation of the circuit is provided in Supplementary Section S2 – Fig. S1, where the initialization, entanglement, and measurement phases are visually depicted.

Finally, the output probability vector is passed to a classical readout function—typically a linear regression model—which maps quantum features to the predicted outcome.

The quantum reservoir evolution can be formally described as:

$$|\Psi(t)>= U(t)|\Psi(t-1)>$$

where:

- $|\Psi(t)>$ is the quantum state at time t.
- $U(t)$ is the unitary operator representing the quantum operations at time t.

This equation signifies the update of the quantum state $|\Psi(t)>$ based on the operator $U(t)$ applied to the previous state $|\Psi(t-1)>$, describing the flow of information through time within the qESN.

2.3. Model training and validation

Both models underwent rigorous training and validation processes:

2.3.1. Training

The models were trained on a subset of the data. For the classic ESN, this involved updating the reservoir states and computing the output weights. The qESN's training involved processing data through quantum circuits and employing classical readout. To isolate and assess the contribution of the reservoir dynamics, both the classical ESN and the qESN employed a simple linear regression as their readout layer. This choice was based on the need to evaluate the internal memory and transformation capabilities of the reservoir, independent of additional nonlinearity introduced by the readout function. While more complex readouts could potentially improve overall performance, they would confound the comparative evaluation of the reservoir's intrinsic processing power. The purpose of this study was to investigate whether quantum reservoirs alone could provide better representation and generalization, particularly under noisy and low-data conditions. Therefore, keeping the readout structure deliberately simple allowed us to attribute performance differences solely to the reservoir, making the comparison between ESN and qESN both more interpretable and rigorous. A broader benchmarking against classical predictors—such as GRU, LSTM, SARIMAX, and Transformer-based architectures—has been addressed in a previous study (Abeltino et al., 2023), where we evaluated the forecasting performance of the Personalized Metabolic Avatar using state-of-the-art time-series models. This prior work focused on classical model architectures, allowing the current study to specifically isolate and quantify the quantum advantage in reservoir dynamics. Future work will explore alternative readouts and optimization strategies to enhance predictive power in production settings, where reservoir-readout co-design can be fully exploited.

2.3.2. Validation

The performance of both models was evaluated using Root Mean Squared Error (RMSE) as the metric. We employed Time Series Cross-Validation (CV) and Walk-Forward Validation (WFV) methods to assess the models' predictive capabilities over unseen data. This approach allowed for a robust assessment of the models in a temporal data context.

2.3.2.1. Cross-Validation.

- Description: CV partitions available data into multiple folds. The model is trained on a subset of data (e.g., 'k-1′ folds) and evaluated on the remaining fold. This process iterates 'k' times, rotating the evaluation fold. It allows the model to be trained and tested on different subsets, offering a comprehensive evaluation. In our application, we performed validation using five distinct data subsets, each progressively increasing in length.

- Utility: This technique effectively utilizes all available data for both training and evaluation, mitigates overfitting risks, and provides a realistic estimation of the model's performance on new, unseen data.

- Validity: CV is considered a valid technique as it assesses the model's performance on data that was not used during training, ensuring a more accurate estimation of the model's generalization to new data.

2.3.2.2. Walk-Forward Validation.

- Description: WFV simulates real-world model use by iteratively training on historical data up to a certain point and then testing on the subsequent data point. This process continues, allowing the model to adapt continually to new data.

- Utility: Particularly suitable for time series problems, this method assesses the model's ability to adapt to new data over time. It evaluates the model's stability and effectiveness in a dynamic context.

- Validity: WFV is considered valid as it evaluates the model's performance at each subsequent time step on unseen data, mimicking real-world model usage in evolving temporal scenarios.

2.4. Computational complexity

The computational complexity of the two models was analyzed in terms of memory usage, training time, and inference cost. For the classical ESN, the main computational cost arises from updating the reservoir states at each timestep and computing the linear regression weights. Given a reservoir of size N and an input of dimension ddd, the state update scales as O(N·d), and training the readout via ridge regression scales as $O(N^2 \cdot T)$, where T is the number of training samples.

In contrast, the qESN uses a quantum reservoir implemented via a simulated quantum circuit. The cost is driven by:

- the number of qubits Q (4 in our case),
- the circuit depth (fixed to 3 layers),
- and the number of shots used to estimate measurement probabilities (set to 1024).

The complexity of simulating a quantum circuit grows exponentially with the number of qubits ($O(2^Q)$), making the simulation cost for 4-qubit systems manageable. However, training the qESN is computationally efficient, as it only requires classical linear regression on the quantum-generated features. Notably, no gradient-based optimization

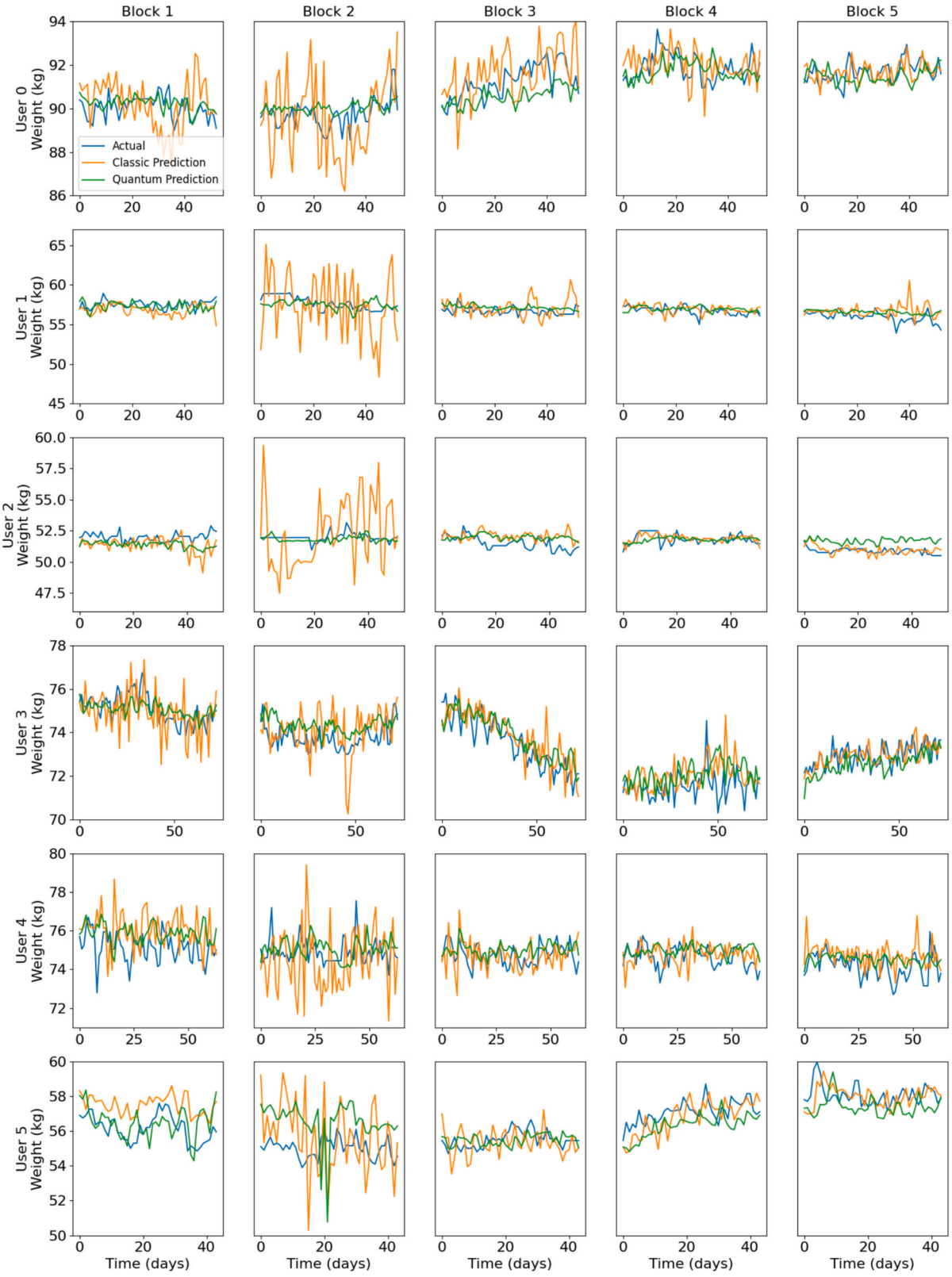

Fig. 2. CV predictions for ESN and qESN models across six users. Each user's predictions are represented by five plots, reflecting predictions for the five temporal blocks within the CV.

or backpropagation is needed, significantly reducing model complexity.

2.5. *Performance evaluation*

The models' performance underwent comprehensive evaluation by comparing the RMSE across both CV and WFV techniques. This

Table 2
Mean RMSE and SD values averaged across 6 users for each of the 5 blocks in the CV process.

Blocks	RMSE Classic CV	RMSE Quantum CV
1	1.20 ± 0.22	0.79 ± 0.24
2	2.21 ± 0.89	0.94 ± 0.52
3	0.98 ± 0.19	0.72 ± 0.12
4	0.77 ± 0.18	0.74 ± 0.18
5	0.71 ± 0.30	0.81 ± 0.18

meticulous comparison aimed to gauge the predictive accuracy and robustness of the models across varying temporal data contexts.

Following the RMSE comparison, we conducted t-tests to statistically ascertain differences between the predictive capabilities of the two models. This statistical analysis provided deeper insights into whether any significant disparities existed in the models' performance metrics. The t-tests were instrumental in quantifying and establishing the statistical significance of observed differences in predictive performance. Our validation process included confirming both normality (Shapiro-Wilk test) and homoscedasticity (Levene test) assumptions necessary for conducting a *t*-test.

2.6. Implementation Considerations

The implementation was carried out using Python, with libraries such as NumPy (version 1.23.5), Pandas (version 1.5.3), Matplotlib (version 3.7.1), and Qiskit (version 0.45.1). These tools provided the necessary functionalities for data manipulation, model development, and QC simulations.

3. Results

Our comprehensive evaluation of ESN across six distinct user time-series datasets has yielded insightful findings, particularly when contrasting the performance of classic ESNs with qESNs. In Table 1, a summary of the results evaluated for each method (CV and WFV) is reported.

During CV, the qESN exhibited superior performance compared to the classic model, showcasing an average RMSE reduction of 31.8 %, corresponding to a delta RMSE of 0.37 (average classic RMSE = 1.18 ± 0.23, average quantum RMSE = 0.80 ± 0.17). Conversely, in WFV, contrasting outcomes were observed. The classic model demonstrated an average RMSE of 0.60 ± 0.12, slightly better than the qESN one (average RMSE of 0.69 ± 0.17), resulting in an RMSE reduction of 15 % for the classic model in this scenario. To further investigate these insights, we carried out a deeper analysis.

3.1. Comparative RMSE scores for cross-validation

To evaluate the performance of both models, a CV procedure was conducted, as elaborated in the preceding section (par. 2.3.2.1). The findings, detailed in Table 1, underscore the superior performance of the quantum model (qESN) over its classical counterpart. At each block, the training dataset size is incremented, starting from 20 % of the total dataset in the first block and reaching 100 % in the final block, increasing by 20 % at each step. Visual inspection of individual predictions for each user across various blocks (refer to Fig. 2) distinctly showcases the comparative underperformance of the ESN, particularly noticeable when the training dataset is limited (first three blocks).

Fig. 2 illustrates the CV predictions for both ESN and qESN across user segments. Notably, the ESN exhibits substantial prediction fluctuations during the initial blocks, whereas qESN demonstrates greater stability in these circumstances. This pattern is further illustrated in Fig. S2, which presents the averaged RMSE across users for the 5 blocks.

Analysis of the ESN's performance (Table 2) reveals heightened variability and inferior outcomes during the early blocks compared to qESN.

Consequently, a detailed assessment was undertaken to ascertain discrepancies between the models across each block. To achieve this, a *t*-test was conducted for individual blocks. The results depicted in Fig. 3 affirm the superiority of qESN, especially when confronted with smaller training datasets.

Notably, as the volume of training data increases, the performance gap between the two models diminishes, rendering their performances comparable.

3.2. Comparative RMSE scores for walk-forward validation

To comprehensively assess the performance of the two models, we conducted WFV, a methodology particularly beneficial when working with temporal data to evaluate model performance in a realistic and dynamic context akin to real-world scenarios (par 2.3.2.2). As shown in Table 1, the initial results suggested comparable performance between the classical and quantum models, a trend further confirmed in Fig. 4, highlighting an advantage for the classical model.

To substantiate this observation, we employed a *t*-test on the two models (see Fig. S3), which confirmed that there is no significant difference between them (p-value > 0.05).

3.3. Comparative RMSE scores with outliers

During the data cleaning phase, apart from handling null values, we also managed potential outliers. Specifically, for User 2, out-of-scale data points were present in the weight time series. During the

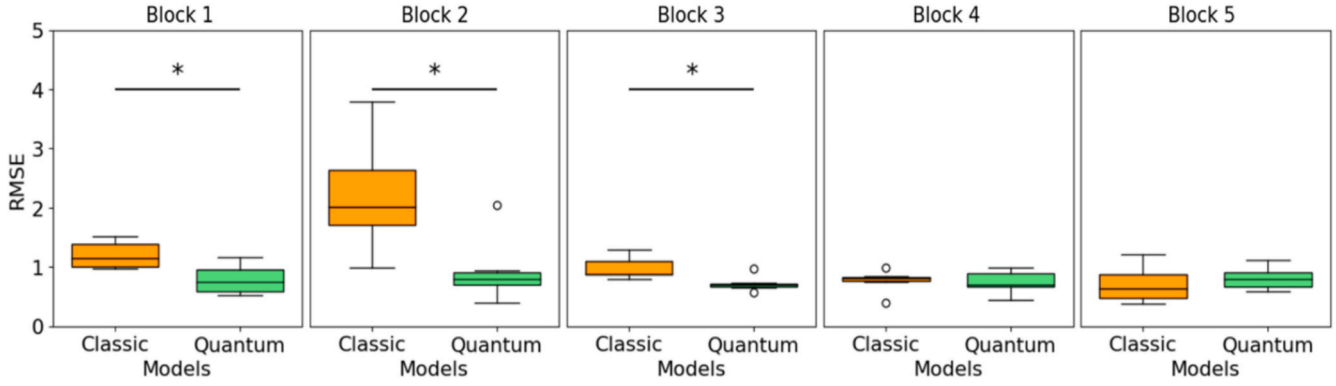

Fig. 3. The figure shows 5 boxplots, each corresponding to a CV block. Each block corresponds to different training data availability: 20%, 40%, 60%, 80%, and 100%. These plots represent the performance of the classic and quantum models. In the first three plots, "*" denotes a significant difference between the two distributions, indicating a substantial distinction between the classic and quantum model performances.

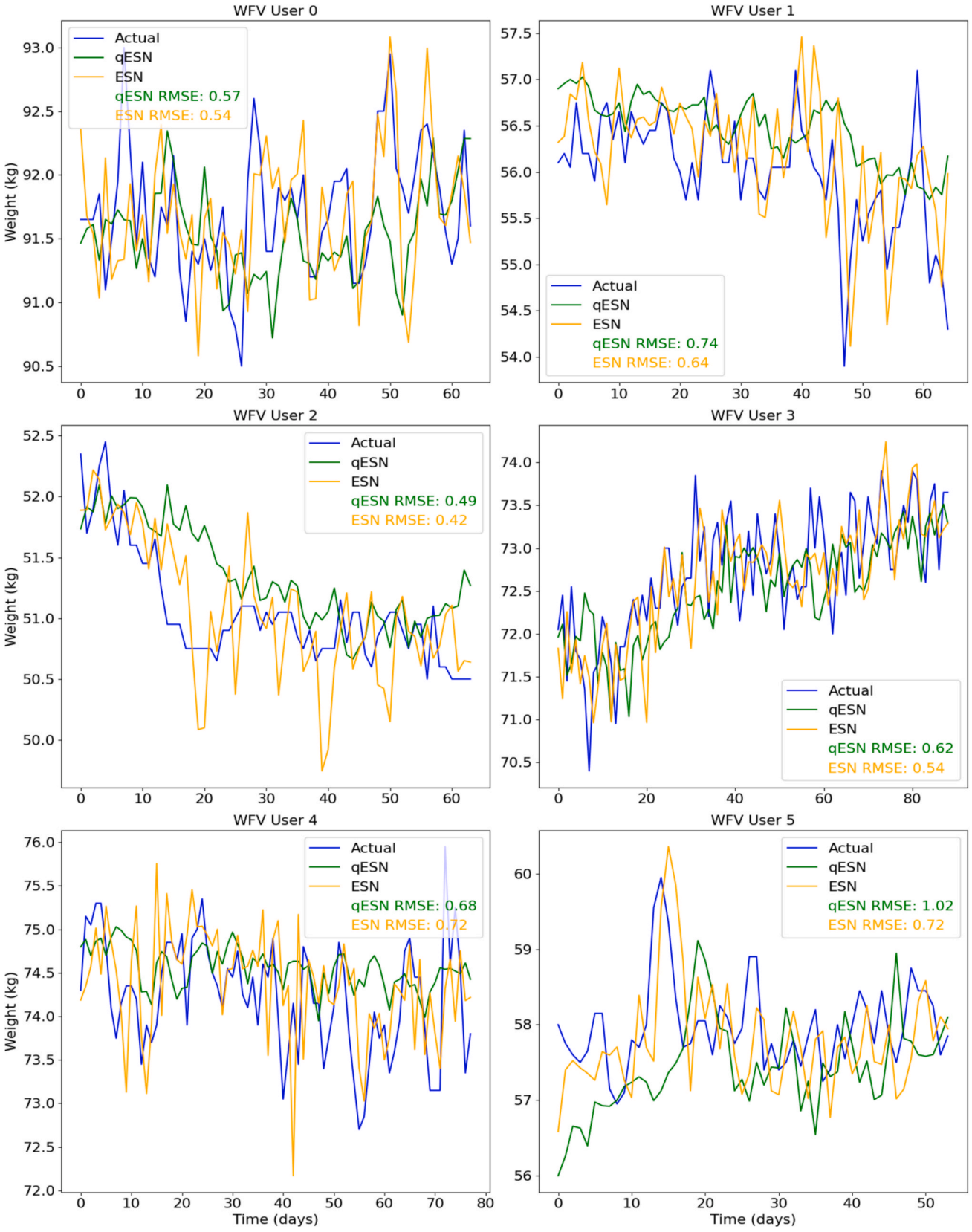

Fig. 4. WFV results illustrating predictions for 6 users using the classic ESN and qESN models.

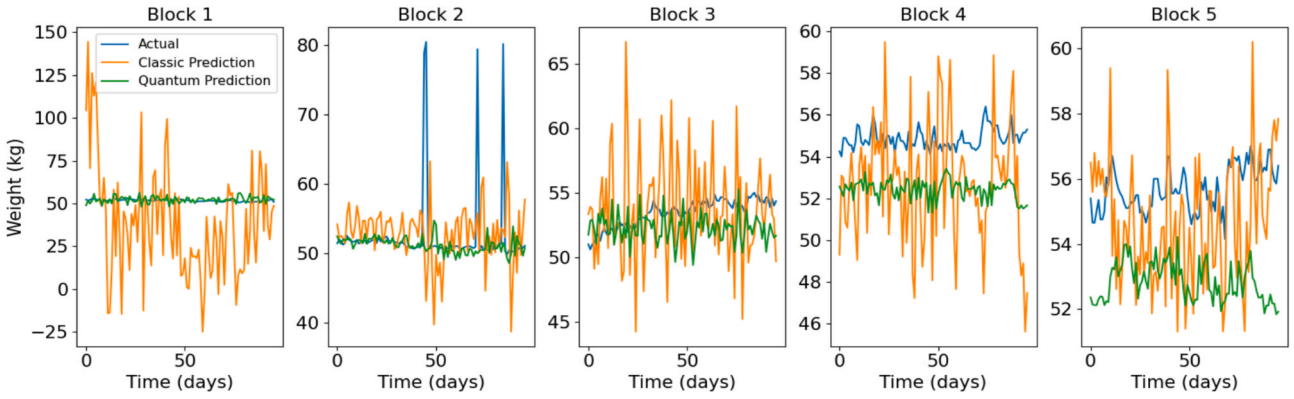

Fig. 5. CV outcomes for User 2, showcasing predictions throughout the 5 validation blocks without outliers' management.

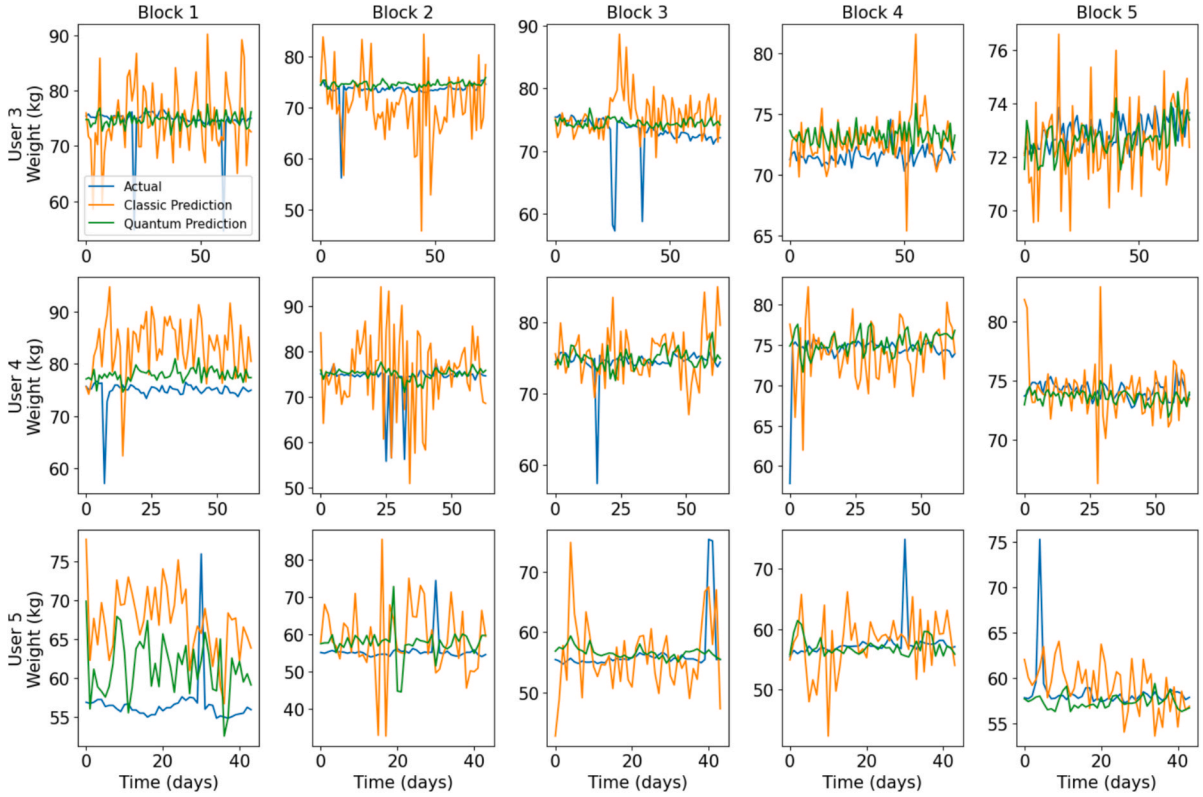

Fig. 6. CV results showcasing the impact of added outliers across three users. Each user's predictions are depicted through five plots, illustrating predictions made for the five temporal blocks within the CV.

Table 3
Average RMSEs for the 5 blocks of the CV.

Blocks	RMSE Classic CV	RMSE Quantum CV
1	7.84 ± 3.53	3.44 ± 1.62
2	22.96 ± 16.08	2.63 ± 1.71
3	8.01 ± 6.08	1.91 ± 0.99
4	4.32 ± 1.66	1.72 ± 0.63
5	2.96 ± 0.94	1.35 ± 0.69

evaluation phase, outliers' management was not considered, leading to unexpected outcomes, as depicted in Fig. 5.

The ESN exhibited considerable challenges, particularly in Block 1 (Fig. 5). The predictions in this block displayed extreme and implausible values, fluctuating between 150 and −25 kg. These predictions notably deviated from the expected range reflected in the actual output, suggesting potential overfitting issues. Conversely, such indications were absent in the qESN's performance. Consequently, we proceeded to analyze the responses of both models when the initial datasets incorporated 8 outliers for each user (reproducing what was observed in the real case of User 2) (Fig. S4).

Executing CV across five blocks (Fig. 6), as previously conducted, revealed notably different results compared to the prior case.

Indeed, in this instance, the qESN outperformed the ESN in both scenarios (Table 3), demonstrating statistical disparities between the two models for each block (Fig. 7).

A similar trend was observed in the WFV, with the qESN consistently exhibiting superior average performance (Fig. 8).

In Fig. 8 it is shown the prediction made for 6 users, the RMSE is averaging reduced far over the 50 % (average classic RMSE = 3.37 ± 1.32, average quantum RMSE = 1.51 ± 0.58), confirming that quantum improve performance with respect the classic also in the WFV.

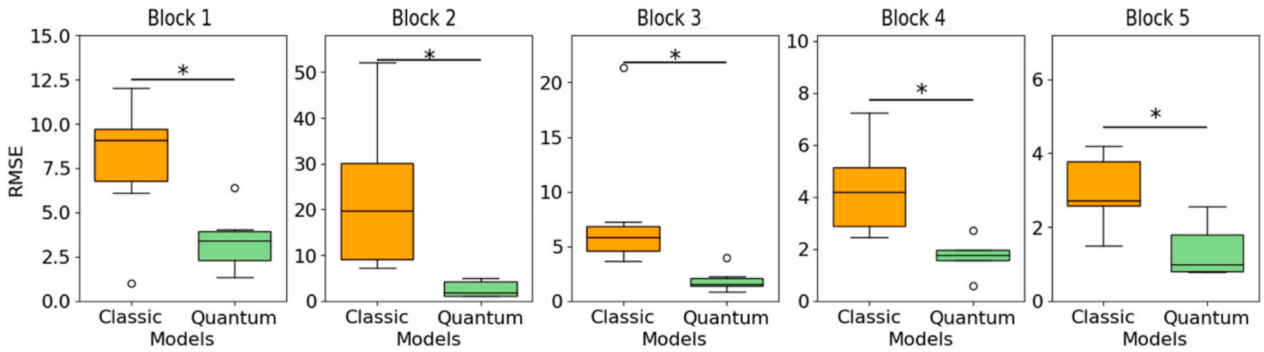

Fig. 7. The figure displays 5 boxplots, each pertaining to a CV block incorporating outliers. These plots illustrate the performance of both classic and quantum models. In the initial three plots, the symbol "*" denotes a significant difference between the two distributions, highlighting a substantial disparity between the classic and quantum model performances.

A *t*-test confirmed statistically the differences observed (Fig. 9), it is noteworthy how the situation has reversed, indicating favorable indicators for the qESN over the classical model in this context.

4. Discussion

The prevalence of obesity and cardiovascular disease remains a critical global health concern largely shaped by dietary habits (Fruh, 2017). The integration of digital health technologies such as wearables and smartphones has facilitated the development of the "Digital Twin", a digital representation of the human body (Ahmadi-Assalemi et al., 2020). Through our dedicated interface (e.g., the ArMOnIApp, as described in section 2.1), we acquired unique data, forming the foundation of the PMA, a model designed to provide customized insights, including individualized responses to dietary adjustments (Abeltino et al., 2023; Abeltino et al., 2022). The clinical significance of the PMA lies in its ability to offer personalized understandings of individual metabolism, thereby promoting healthier lifestyles.

Quantum implementation presents promising prospects in advancing the PMA, potentially amplifying its precision and predictive capabilities. This advancement could lead to more accurate and tailored recommendations for individuals' dietary and physical activity responses. The discernible superiority of the qESN over the classic ESN aligns seamlessly with the burgeoning literature advocating for the integration of quantum algorithms. This integration consistently enhances computational efficiency and augments predictive accuracy.

Drawing from the pioneering work by Fujii and Nakajima (2017) (Fujii and Nakajima, 2017), which initially introduced the concept of QRC, our qESN model unveils an augmented memory capacity. This feature proves pivotal for tasks mandating the retention and processing of historical information to forecast future states accurately.

The study's revelations bring to the fore the nuanced performance disparities between the qESN and the classic ESN across diverse scenarios. While both models demonstrate comparable proficiency under ideal circumstances, the quantum model distinctly outshines its classical counterpart when trained on limited data. Indeed, qESN showed a more suitable response in real applications where data availability is restricted. For the first three blocks of the CV, with training set lengths of 70 ± 11, 140 ± 22, and 210 ± 34 days respectively, the qESN showed an RMSE reduction over the classical model of 34.85 ± 12.80 %, 50.60 ± 28.23 %, and 25.64 ± 11.49 % (Table 2). These findings validate the efficacy of quantum algorithms in managing data scarcity, providing a compelling advantage in time series forecasting under constrained conditions.

Moreover, the qESN's resilience to outliers, a salient facet emphasized in this study, significantly contributes to its consistent superior performance across multifaceted contexts. Notably, the model's robustness against outliers not only augments predictive accuracy but also amplifies its efficacy in scenarios where classical models encounter setbacks due to data irregularities. In two test conditions, one without and one with artificially introduced outliers, the improvement brought by qESN compared to the classical version increased from 32 % to 76 %. This was due both to a substantial degradation in ESN performance and to the stability of qESN, which experienced a moderate RMSE deterioration (51.16 ± 25.36 %) compared to the more pronounced decline in the classical ESN (70.56 ± 31.87 %).

Furthermore, the integration of these findings into the WFV analysis substantiates the quantum model's superiority, especially in scenarios affected by data outliers. The WFV highlighted a shift from a slight classical advantage (approximately 15 % improvement) in clean data to a clear quantum advantage (55 % improvement) in the presence of outliers. As observed in the CV, this inversion is driven by the qESN's capacity to maintain stable performance in the presence of noise (RMSE decrease of 47.02 ± 23.09 %) compared to the higher sensitivity of the classical ESN (RMSE increase of 78.66 ± 10.33 %). This holistic validation underscores the adaptability and continual learning potential of quantum machine learning models in dynamic real-time forecasting settings, accentuating their paramount significance in applications requiring adaptation to evolving data streams. Importantly, our study employed a linear regression readout for both models to ensure that performance differences could be attributed solely to the reservoir architecture. While more complex optimizers might enhance predictive accuracy, our choice supports a clean comparison of the information processing capabilities intrinsic to quantum versus classical reservoirs. This minimal design further reinforces the potential of qESN as a lightweight, interpretable model in data-constrained environments.

From a translational perspective, the Quantum Metabolic Avatar (QMA) offers substantial potential in clinical and health-technology domains. Its ability to model personalized metabolic responses using minimal and potentially noisy data renders it particularly suitable for deployment in mobile health (mHealth) environments, including wearable-based monitoring platforms. In these scenarios, the lightweight structure and training-free inference of qESNs enable near-real-time prediction and adaptability, which are essential in guiding dietary and behavioral interventions. Furthermore, in research on rare metabolic disorders or early-phase interventions where large datasets are often unavailable, the demonstrated generalization capacity of qESNs provides a pragmatic advantage for modeling and decision support. This approach aligns with the broader vision of digital twins in precision medicine, offering scalable and individualized modeling tools that operate effectively even in underdetermined conditions.

However, the study does acknowledge certain limitations. The intricate nature and nascent stage of quantum algorithms imply that several practical challenges persist. The existing hardware constraints of quantum processors may limit the scalability and direct deployment of the approach in current clinical settings. A further limitation of both

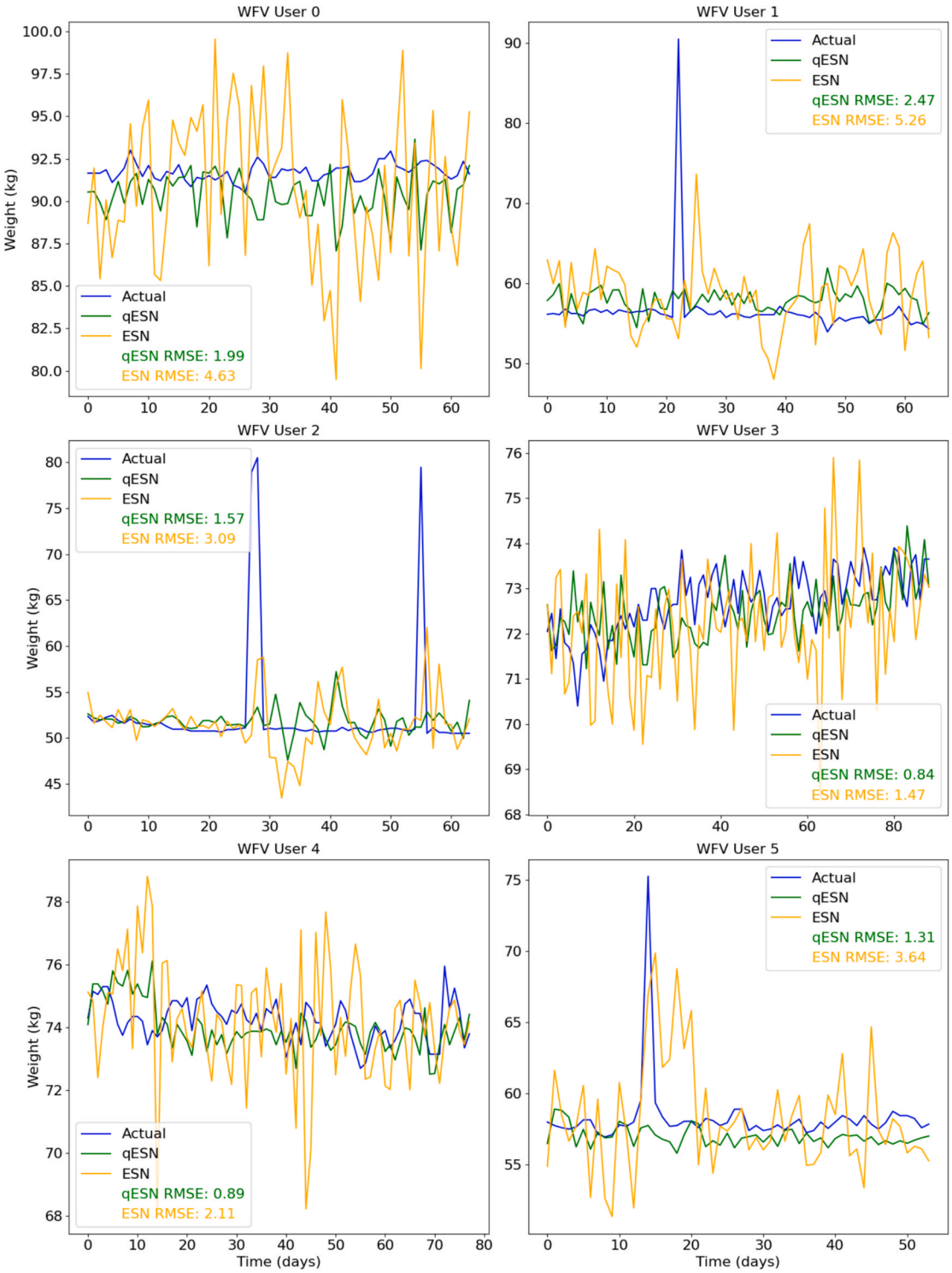

Fig. 8. WFV results illustrating predictions for 6 users using the classic ESN and qESN models.

QMA and PMA lies in their individual-centric design, which does not yet support generalized inference across multiple users. To address this, we recently developed the Generalized Metabolic Avatar (GMA) (Abeltino et al., 2025) a classical ensemble-based model that incorporates demographic parameters to forecast weight changes without requiring personalized historical data. Given the promising results obtained with the QMA, we foresee an extension of the GMA into its quantum version, potentially combining the generalization capacity of GMA with the quantum-enhanced robustness and memory of qESN-based architectures.

5. Conclusion

Our research contributes significantly to the emerging evidence supporting the prowess of quantum machine learning, particularly qESNs, in surpassing classical algorithms for specific tasks. As the field continues to mature and quantum hardware advances in accessibility and power, we anticipate that the advantages observed in this study will

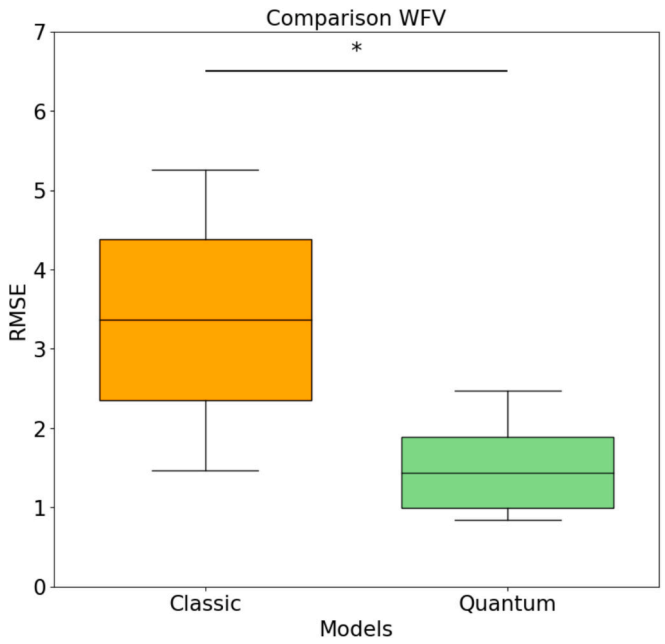

Fig. 9. The figure shows the outcomes of the WFV through a comparative boxplot analysis between the quantum and classical models. The symbol "*" signifies a statistical difference between the two distributions, highlighting a better performance of the qESN with respect to the classic ESN.

accentuate further. This trajectory positions quantum machine learning to revolutionize diverse fields by offering heightened predictive capabilities and innovative applications. Another crucial facet of ongoing research entails unraveling the intricate interplay between the network's memory capacity and its hyperparameters. This investigation stands pivotal in realizing the full potential of qESN, particularly in optimizing their efficacy for specific applications. Moreover, the domain grapples with the intricate task of deploying these networks on Noisy Intermediate-Scale Quantum (NISQ) computers (Cheng et al., 2023) a significant barrier that demands resolution to render quantum machine learning a feasible reality.

These outcomes pave the way for new applications across diverse fields, such as analyzing metabolism-related data like nutrigenomics or the microbiome (Bianchetti et al., 2023; Abeltino et al., 2024) offering insights into micro and macro-reactions within our metabolism. In the realm of developing algorithms to detect time series data related to human body responses—such as heart rate (Serantoni et al., 2022; Dong et al., 2013) innovative analyses like chewing patterns (Riente et al., 2023), QC can catalyze new developments by addressing common challenges prevalent in these applications. Building upon these findings, QC will play an essential role in new crafting models capable of estimating the likelihood of encountering specific pathologies, such as those associated with type 2 diabetes (Bianchetti et al., 2023; Bianchetti et al., 2023; Bianchetti et al., 2022; Bianchetti et al., 2022).

In conclusion, the current study sets the stage for the promising future of quantum machine learning in unraveling complexities across diverse disciplines. The anticipated advancements in quantum algorithms and hardware stand poised to catalyze transformative breakthroughs, facilitating a deeper understanding of intricate biological mechanisms, and fostering precision medicine paradigms.

CRediT authorship contribution statement

A. Abeltino: Conceptualization, Methodology, Software, Validation, Formal analysis, Investigation, Resources, Data curation, Writing – original draft, Visualization. **C. Serantoni:** Methodology, Formal analysis, Investigation, Writing – review & editing. **M.M. De Giulio:** Conceptualization, Methodology, Validation, Formal analysis, Investigation, Writing – review & editing, Visualization. **A. Riente:** Methodology, Validation, Formal analysis, Investigation. **S. Capezzone:** Methodology, Validation, Investigation. **R. Esposito:** Methodology, Validation. **M. De Spirito:** Methodology, Investigation. **G. Maulucci:** Conceptualization, Methodology, Software, Validation, Formal analysis, Investigation, Resources, Data curation, Writing – original draft, Writing – review & editing, Supervision, Project administration, Funding acquisition.

Funding

This project was supported in part by two research grants awarded to GM from Regione Lazio PO FSE 2014–2020 "Intervento per il rafforzamento della ricerca nel Lazio—incentivi per i dottorati di innovazione per le imprese", one cofunded by RAN Innovation (2021) and another co-funded by BLUSISTEMI S.R.L. (2022), and by a research grant awarded to GM by Università Cattolica del Sacro Cuore-Linea D1 2021.

Declaration of competing interest

The authors declare the following financial interests/personal relationships which may be considered as potential competing interests: Giuseppe Maulucci reports financial support was provided by Lazio Region. Giuseppe Maulucci reports financial support was provided by RAN innovation.

Acknowledgments

Institutional Review Board Statement.

This study was conducted in accordance with the Declaration of Helsinki and approved by the Ethics Committee of Università Cattolica del Sacro Cuore (Protocol Code diab_mf, 16 March 2017).

Informed Consent Statement.

Informed consent was obtained from all subjects involved in this study. Written informed consent to publish this paper has been obtained from the participants.

Conflicts of Interest.

The authors declare no conflict of interest.

Appendix A. Supplementary data

Supplementary data to this article can be found online at https://doi.org/10.1016/j.eswa.2025.129045.

Data availability

Data and codes are available upon reasonable request

References

Biamonte, J., Wittek, P., Pancotti, N., Rebentrost, P., Wiebe, N., & Lloyd, S. (2017). Quantum machine learning. *Nature, 549*, 195–202. https://doi.org/10.1038/nature23474

Liu, J., Sun, T., Luo, Y., Yang, S., Cao, Y., & Zhai, J. (2020). An echo state network architecture based on quantum logic gate and its optimization. *Neurocomputing, 371*, 100–107. https://doi.org/10.1016/j.neucom.2019.09.002

Fujii, K., & Nakajima, K. (2021:). Quantum Reservoir Computing: A Reservoir Approach Toward Quantum Machine Learning on Near-Term Quantum Devices. *in*, 423–450. https://doi.org/10.1007/978-981-13-1687-6_18

Suzuki, Y., Gao, Q., Pradel, K. C., Yasuoka, K., & Yamamoto, N. (2022). Natural quantum reservoir computing for temporal information processing. *Sci. Rep., 12*, 1353. https://doi.org/10.1038/s41598-022-05061-w

Fujii, K., & Nakajima, K. (2017). Harnessing Disordered-Ensemble Quantum Dynamics for Machine Learning. *Physics Review Appl., 8*, Article 024030. https://doi.org/10.1103/PhysRevApplied.8.024030

Molteni, R., Destri, C., & Prati, E. (2023). Optimization of the memory reset rate of a quantum echo-state network for time sequential tasks. *Physics Letters A, 465*, Article 128713. https://doi.org/10.1016/j.physleta.2023.128713

Yao, X., Shao, Y., Fan, S., & Cao, S. (2022). Echo state network with multiple delayed outputs for multiple delayed time series prediction. *Journal of the Franklin Institute, 359*, 11089–11107. https://doi.org/10.1016/j.jfranklin.2022.09.059

Yao, X., Wang, Y., Ma, D., Cao, S., & Ma, Q. (2024). Fractional-integer-order echo state network for time series prediction. *Appl Soft Comput, 153*. https://doi.org/10.1016/j.asoc.2024.111289

Kobayashi, M., Nakaji, K., & Yamamoto, N. (2022). Overfitting in quantum machine learning and entangling dropout. *Quantum Mach Intell, 4*, 30. https://doi.org/10.1007/s42484-022-00087-9

Caro, M. C., Huang, H.-Y., Cerezo, M., Sharma, K., Sornborger, A., Cincio, L., & Coles, P. J. (2022). Generalization in quantum machine learning from few training data. *Nat Commun, 13*, 4919. https://doi.org/10.1038/s41467-022-32550-3

Abeltino, A., Bianchetti, G., Serantoni, C., Riente, A., De Spirito, M., & Maulucci, G. (2023). Putting the Personalized Metabolic Avatar into production: A Comparison between Deep-Learning and Statistical Models for Weight Prediction. *Nutrients, 15*. https://doi.org/10.3390/nu15051199

Abeltino, A., Bianchetti, G., Serantoni, C., Ardito, C. F., Malta, D., De Spirito, M., & Maulucci, G. (2022). Personalized Metabolic Avatar: A Data Driven Model of Metabolism for Weight Variation forecasting and Diet Plan Evaluation. *Nutrients, 14*. https://doi.org/10.3390/nu14173520

Bianchetti, G., Abeltino, A., Serantoni, C., Ardito, F., Malta, D., De Spirito, M., & Maulucci, G. (2022). Personalized Self-monitoring of Energy Balance through Integration in a Web-Application of Dietary, Anthropometric, and Physical activity Data. *J Pers Med, 12*. https://doi.org/10.3390/jpm12040568

Abeltino, A., Serantoni, C., Riente, A., De Giulio, M., Capezzone, S., Esposito, R., De Spirito, M., & Maulucci, G. (2025). Transforming personalized weight forecasting: From the Personalized Metabolic Avatar to the Generalized Metabolic Avatar. *Comput Biol Med, 188*. https://doi.org/10.1016/j.compbiomed.2025.109879

Cui, H., Liu, X., & Li, L. (2012). The architecture of dynamic reservoir in the echo state network, Chaos: An Interdisciplinary. *Journal of Nonlinear Science, 22*. https://doi.org/10.1063/1.4746765

Ma, Q., Shen, L., Chen, W., Wang, J., Wei, J., & Yu, Z. (2016). Functional echo state network for time series classification. *Inf Sci (N Y), 373*, 1–20. https://doi.org/10.1016/j.ins.2016.08.081

Fruh, S. M. (2017). Obesity. *J Am Assoc Nurse Pract, 29*, S3–S14. https://doi.org/10.1002/2327-6924.12510

Ahmadi-Assalemi, G., Al-Khateeb, H., Maple, C., Epiphaniou, G., Alhaboby, Z. A., Alkaabi, S., & Alhaboby, D. (2020). Digital twins for precision healthcare. In *Advanced Sciences and Technologies for Security Applications* (pp. 133–158). Springer. https://doi.org/10.1007/978-3-030-35746-7_8.

Cheng, B., Deng, X.-H., Gu, X., He, Y., Hu, G., Huang, P., Li, J., Lin, B.-C., Lu, D., Lu, Y., Qiu, C., Wang, H., Xin, T., Yu, S., Yung, M.-H., Zeng, J., Zhang, S., Zhong, Y., Peng, X., Nori, F., & Yu, D. (2023). Noisy intermediate-scale quantum computers. *Front Phys (Beijing), 18*, 21308. https://doi.org/10.1007/s11467-022-1249-z

Bianchetti, G., De Maio, F., Abeltino, A., Serantoni, C., Riente, A., Santarelli, G., Sanguinetti, M., Delogu, G., Martinoli, R., Barbaresi, S., De Spirito, M., & Maulucci, G. (2023). Unraveling the Gut Microbiome–Diet connection: Exploring the Impact of Digital Precision and Personalized Nutrition on Microbiota Composition and Host Physiology. *Nutrients, 15*, 3931. https://doi.org/10.3390/nu15183931

Abeltino, A., Hatem, D., Serantoni, C., Riente, A., De Giulio, M. M., De Spirito, M., De Maio, F., & Maulucci, G. (2024). Unraveling the Gut Microbiota: Implications for Precision Nutrition and Personalized Medicine. *Nutrients, 16*. https://doi.org/10.3390/nu16223806

Serantoni, C., Zimatore, G., Bianchetti, G., Abeltino, A., De Spirito, M., & Maulucci, G. (2022). Unsupervised Clustering of Heartbeat Dynamics Allows for Real Time and Personalized Improvement in Cardiovascular Fitness. *Sensors, 22*, 3974. https://doi.org/10.3390/s22113974

Y. Dong, J. Scisco, M. Wilson, E. Muth, A. Hoover, Detecting Periods of Eating During Free-Living by Tracking Wrist Motion, 2013. http://www.apple.com/iPhone/.

Riente, A., Abeltino, A., Serantoni, C., Bianchetti, G., De Spirito, M., Capezzone, S., Esposito, R., & Maulucci, G. (2023). Evaluation of the Chewing Pattern through an Electromyographic Device. *Biosensors (Basel), 13*. https://doi.org/10.3390/bios13070749

Bianchetti, G., Cefalo, C. M. A., Ferreri, C., Sansone, A., Vitale, M., Serantoni, C., Abeltino, A., Mezza, T., Ferraro, P. M., De Spirito, M., Riccardi, G., Giaccari, A., & Maulucci, G. (2023). Erythrocyte membrane fluidity: A novel biomarker of residual cardiovascular risk in type 2 diabetes. *Eur J Clin Invest*. https://doi.org/10.1111/eci.14121

Bianchetti, G., Clementi, M. E., Sampaolese, B., Serantoni, C., Abeltino, A., De Spirito, M., Sasson, S., & Maulucci, G. (2023). Metabolic Imaging and Molecular Biology Reveal the Interplay between Lipid Metabolism and DHA-Induced Modulation of Redox Homeostasis in RPE Cells. *Antioxidants, 12*, 339. https://doi.org/10.3390/antiox12020339

Bianchetti, G., Rizzo, G. E., Serantoni, C., Abeltino, A., Rizzi, A., Tartaglione, L., Caputo, S., Flex, A., De Spirito, M., Pitocco, D., & Maulucci, G. (2022). Spatial Reorganization of Liquid Crystalline Domains of Red Blood Cells in Type 2 Diabetic patients with Peripheral Artery Disease. *Int J Mol Sci, 23*, 11126. https://doi.org/10.3390/ijms231911126

Bianchetti, G., Clementi, M. E., Sampaolese, B., Serantoni, C., Abeltino, A., De Spirito, M., Sasson, S., & Maulucci, G. (2022). Investigation of DHA-Induced Regulation of Redox Homeostasis in Retinal Pigment Epithelium Cells through the Combination of Metabolic Imaging and Molecular Biology. *Antioxidants, 11*, 1072. https://doi.org/10.3390/antiox11061072